Biophysical Journal Volume 106 June 2014 2667–2674

Rigidity, Secondary Structure, and the Universality of the Boson Peak in Proteins

Stefania Perticaroli,[†‡§] Jonathan D. Nickels,[†§*] Georg Ehlers,[¶] and Alexei P. Sokolov[†‡§]
[†]Joint Institute for Neutron Sciences and [‡]Chemical and Materials Sciences Division, Oak Ridge National Laboratory, Oak Ridge, Tennessee; [§]Department of Chemistry, University of Tennessee, Knoxville, Tennessee; and [¶]Quantum Condensed Matter Division, Oak Ridge National Laboratory, Oak Ridge, Tennessee

ABSTRACT Complementary neutron- and light-scattering results on nine proteins and amino acids reveal the role of rigidity and secondary structure in determining the time- and lengthscales of low-frequency collective vibrational dynamics in proteins. These dynamics manifest in a spectral feature, known as the boson peak (BP), which is common to all disordered materials. We demonstrate that BP position scales systematically with structural motifs, reflecting local rigidity: disordered proteins appear softer than α-helical proteins; which are softer than β-sheet proteins. Our analysis also reveals a universal spectral shape of the BP in proteins and amino acid mixtures; superimposable on the shape observed in typical glasses. Uniformity in the underlying physical mechanism, independent of the specific chemical composition, connects the BP vibrations to nanometer-scale heterogeneities, providing an experimental benchmark for coarse-grained simulations, structure/rigidity relationships, and engineering of proteins for novel applications.

INTRODUCTION

Protein dynamics span from subpicosecond vibrations to large domain motions occurring on the micro- and millisecond timescales. And although functional motions in enzymes are understood to be rate-limited by these large-amplitude motions; it was recently demonstrated that subpicosecond vibrational motions may play a crucial role in the function of biomolecules, promoting enzyme-catalyzed reactions (1), chemical barrier crossing (2,3), and proton tunneling effects (4,5). Indeed, some transition states are characterized by lifetimes on the order of tens of femtoseconds (3), comparable to the timescale of low-frequency collective vibrations of proteins. It was even suggested in a recent molecular dynamics study (6) that such motions facilitate large conformational translations. Protein function is encoded in its structure, which defines the dynamics and mechanical properties of the protein (7–9). Based on these building blocks, we arrive at the diverse range of biological materials, such as skin, bone, hair, titin, and spider silk, all with highly specific mechanical properties casually assigned to secondary structure (7–9). The α-helical motif, for instance, provides mechanical stability to cells and plays a fundamental role in biophysical processes involving mechanical signaling, whereas the β-sheets forming domains that constitute silks, muscle tissue, and amyloid fibrils promote toughness and strength.

Proteins and glass formers share a wide range of dynamical features (10), among which the boson peak (BP) has been one of the most widely debated. The BP is a spectral feature in neutron and light scattering in the range~2–7 meV (~16–45 cm^{-1}) found in proteins (11–18) and glasses (19–26). It is connected to the vibrational density of states, $g(\nu)$, in excess of the expected Debye level ($g_D(\nu) \propto \nu^2$). The BP appears in the energy range where the acoustic phonons have a wavelength on the order of a few nanometers, a typical lengthscale at which the continuum elastic description valid for crystalline systems breaks down in glasses (27). Several studies have shown a strong correlation between the BP and acoustic modes in glass formers (27,28). Despite these efforts, the microscopic origin of the BP is still debated. Soft-potential models connect the BP to quasi-local vibrational modes, which coexist and hybridize with the sound waves at the BP energy (29–31). Another approach relates the BP of a glass to the softened and broadened (due to structural disorder) transverse acoustic singularity of the relevant crystal (32). Random first-order transition theory relates the BP to motions of domain walls that separate cooperatively rearranging regions (33,34). And yet other models ascribe the BP to structural heterogeneity, which results in a spatial distribution of local elastic constants (35–38), or to strong phonon localization within nanoscale domains. These approaches relate the BP to the size and properties of such heterogeneities (39–42).

There is an opportunity to use this heterogeneity approach to overlap with structural biology. The secondary structures of proteins are defined as the local spatial arrangement of the peptide backbone, stabilized by interactions such as hydrogen bonds and solvent exclusion. Typically, this is described by well-defined motifs such as α-helices, β-strands, turns, or loops. The lengthscale of secondary structural units (~1−4 nm) is on the order of the nanoscopic heterogeneities known in glasses.

Submitted February 24, 2014, and accepted for publication May 7, 2014.
*Correspondence: nickelsjd@ornl.gov
Stefania Pericaroli and Jonathan D. Nickels contributed equally to this work.
Editor: Lois Pollack.

0006-3495/14/06/2667/8 $2.00
http://dx.doi.org/10.1016/j.bpj.2014.05.009

Microscopically, the BP in proteins is thought to contain contributions from a range of collective vibrational modes. These motions are distributed throughout the molecule (12,13), including in the backbone and polar and nonpolar side chains (12). Although these modes might be collective, only a minority of the scattered intensity at the BP can be connected to in-phase motions of secondary structural units, as demonstrated by coherent-NS measurements of the BP in green fluorescent protein (GFP) (43).

In this work, we report the insights gained from observations of the BP in several proteins and amino acids, analyzing both peak position and spectral shape. Our analysis reveals a trend of increasing BP frequency with increasing rigidity of the predominant secondary structure of the protein, with random coils being softer than α-helices and β-sheets being the most rigid structure we studied. There also appears to be a surprising universality of the spectral shape of the BP for all the proteins and even the amino acid mixtures studied here. The spectral shape of the BP in proteins is essentially the same as what has been observed in a wide range of glass formers (23). We interpret these results in terms of the nanoheterogeneities model proposed for glasses (39–42). The correlation length-scales ($\xi = 1.8$–2.4 nm) estimated in this approach appear to be comparable with the size of secondary structural elements, such as the length of α-helices and of β-sheets (16).

RESULTS AND DISCUSSION

We have used both neutron scattering (NS) and depolarized light scattering (LS) experiments to measure the BP in dry, lyophilized protein powders at 170 K and 295 K. The NS experiments were performed on the Cold Neutron Chopper Spectrometer (44) at the Spallation Neutron Source (SNS) at Oak Ridge National Laboratory (Oak Ridge, TN). Detailed descriptions of the NS, depolarized LS, and complementary measurements using Brillouin, Fourier transform infrared spectroscopies, and refractive index data are provided in the Supporting Material and previous work (16). We chose seven model proteins to isolate secondary structures found in native proteins: β-sheets (concanavalin A (CON) and immunoglobulin G (IgG)), β-barrel (GFP), $\alpha+\beta$ structure (lysozyme (LYS)), α-helices (myoglobin (MYO) and bovine serum albumin (BSA)), and intrinsically disordered proteins (β-casein (CAS)). The relative content of each secondary structure for the model proteins, as defined by mass fraction, is reported in Table S1 in the Supporting Material. To test the sensitivity of the BP to chemical composition, as well as the presence of the polypeptide backbone and particular secondary structure, we also analyzed two amino acid mixtures that reproduce the amino acid compositions of GFP and BSA (aa-GFP and aa-BSA, respectively; for details, see Table S2). The secondary structures of all the proteins and the absence of polypeptide chain in the aa-mixtures were directly confirmed by Fourier transform infrared spectroscopy measurements of the amide region (1400–1700 cm^{-1}) (Fig. S1).

BP position

Fig. 1 *a* shows the NS spectra of seven different proteins, together with the aa-GFP mixture, at 170 K in the spectral density formalism, $I_n(\nu)$, for both depolarized LS and NS data. Depolarized LS spectra correspond to the energy-loss side, and therefore the expression used to obtain the spectral density was

$$I_n^{LS} = \frac{I(\nu)}{\nu \times [n_B(\nu) + 1]}, \quad (1)$$

where $I(\nu)$ is the measured intensity and

$$n_B(\nu) = [\exp(h\nu/kT) - 1]^{-1}, \quad (2)$$

is the Bose-Einstein occupation number.

NS spectra were collected in the energy-gain side, although they are shown here with a positive energy axis

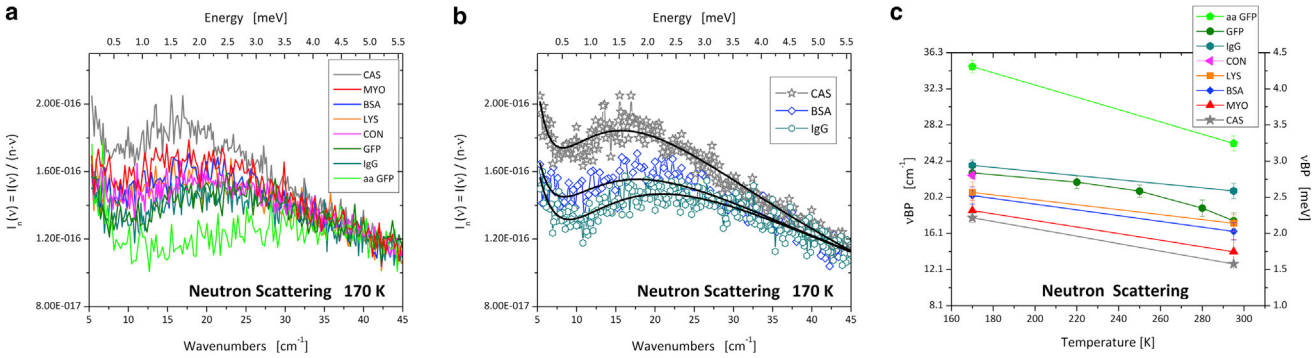

FIGURE 1 (*a*) NS spectra in the BP region presented as the spectral density for the seven dry proteins and aa-GFP mixture. The spectra have been normalized at the high-frequency tail. (*b*) NS spectra of β-casein (*gray stars*), BSA (*blue diamonds*), and IgG (*teal hexagons*) representative of random coil, α-helix, and β-sheet secondary structures. Solid black lines present the fit using Eq. 1. (*c*) BP frequencies obtained from the NS data plotted versus temperature. Lines serve as a guide for the eye. Experimental points at 170 and 295 K are shown for all samples, and additional points at 220, 250, and 280 K are shown for GFP. The error bars are the uncertainties provided by the fit. To see this figure in color, go online.

for comparison to LS spectra; consequently, $I_n(\nu)$ was calculated according to the equation

$$I_n^{NS}(\nu) = \frac{I(\nu)}{\nu \times n_B(\nu)}. \quad (3)$$

The NS spectra used for this presentation were summed over all measured Q (0.5–5 $Å^{-1}$), because no significant Q dependence of the spectral shape was observed, and subsequently normalized at the high-frequency tail (16). There is an increase in the frequency of the BP going from β-casein to aa-GFP, indicating a progressive stiffening of the systems.

To quantitatively compare the BP frequency, ν_{BP}, for the different samples, we fit the spectral densities of the samples according to the expression (16)

$$I_n(\nu) = \frac{A}{\nu^2 + \nu_0^2} + B \times \exp\left[-\frac{\left(\ln\frac{\nu}{\nu_{BP}}\right)^2}{2W^2}\right] + y_0, \quad (4)$$

where the first term accounts for the quasielastic scattering contribution approximated by a Lorentzian function with width ν_0 and amplitude A, and the second term describes the BP in terms of a lognormal function (24) of width W and amplitude B. This procedure was used for both NS and LS data sets. In the case of NS data, the background parameter y_0 was 0. This parameter was left free in the case of LS to account for possible photoluminescence contribution. Representative fits are shown in Fig. 1 *b* for the various structural classes, intrinsically disordered (CAS) and α- (BSA) and β-proteins. The temperature evolution of ν_{BP} for all samples measured with NS are plotted in Fig. 1 *c*. LS data are consistent with NS results, and the ν_{BP} from LS is reported together with the NS data at 295 K in Fig. S5. We observe the same trend in the rigidity of the proteins at each temperature, going from disordered protein to α-helices to β-structures, with the amino acid mixture appearing the most stiff: CAS < MYO < BSA < LYS < CON < GFP < IgG < aa-GFP (Fig. 1 *c*). This correlation is presented in the context of the secondary structure in Fig. 2. Both β-sheets and β-barrels are more rigid structural units than α-helices, consistent with our previous work conducted on four model proteins (16). Lysozyme with α- and β-structures appears to have moderate rigidity between α- and β-structures; and finally casein, with its intrinsically disordered structure, is the softest protein observed in this study.

In a previous investigation (16), it was suggested that the microscopic reason for the higher rigidity of the β-barrel GFP might be related to its higher number of hydrogen bonds per residue relative to the α-helices in MYO and BSA. Here, the expanded data set, including β-sheet proteins (CON and IgG), allows us to point out that high rigidity appears to be a general property of β-structures and not exclusively an effect of extra mechanical stability due to the barrel configuration. This expanded data set also allows for more definitive comment on the proposed elastic global model (45). We present the molecular masses and the hydrodynamic radii (R_H) of the proteins in Table 1 (46–51) and Fig. S6. According to the elastic global model (45), the BP position should scale with the inverse R_H. Our results (Table 1) clearly demonstrate that the BP position does not scale with the size of the biomolecule, illustrating the shortcomings of this model.

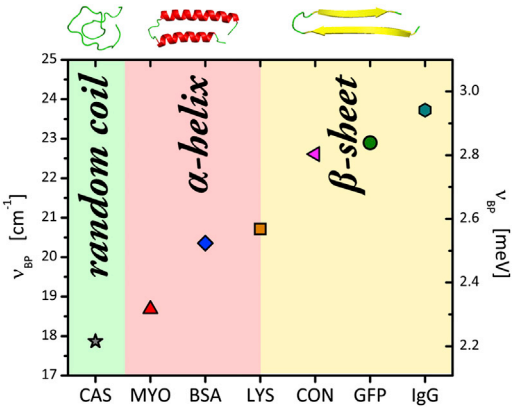

FIGURE 2 Correlation between frequency of the BP and rigidity of different secondary structures of proteins. Order of increasing rigidity: random coil < α-helix < β-sheet. Results obtained from NS data on dry powders at 170 K. To see this figure in color, go online.

The inclusion of a disordered protein, β-casein, in this data set is significant in two ways: first in the context of the biological and nanomaterial relevance, and second as a link through which we can compare our results to the BP properties of random-coil structures of synthetic polymers. It is clear that the relative softness of the BP in CAS is consistent with the large plasticity of intrinsically disordered proteins due to their lack of rigid folded structure, which allows these proteins to interact with many different targets (52).

Fig. 3 *a* presents depolarized LS spectra of dry aa-mixtures representing the composition of GFP and BSA (aa-GFP and aa-BSA), again as spectral density at 170 K and 295 K. The BP is clearly observed for both aa-mixtures, as was anticipated by Diehl et al. (11), and recently demonstrated by Schirò et al. (53) for an aa-mixture representing the composition of myoglobin. At each observed temperature, the BPs of aa-BSA and aa-GFP appear to be superimposable; suggesting that the position and shape of the peak are not sensitive to the change in composition of amino acids for these two samples (compositions shown in Table S2). Fig. 3 *b* presents a comparison of the NS spectra of aa-GFP (*solid lines*) and the protein GFP (*symbols*) at 170 K. This is not the same comparison of amino acids as in Fig. 3 *a*, but a comparison of the aa-mixture to the protein with the same chemical composition. The BP of the

TABLE 1 Model parameters

	ν_{BP} (meV)	Molecular mass (kDa)	R_H (nm)	ξ (nm)	Average length or width (nm)
MYO	2.32 ($\pm$ 0.14)	17.8	2.12 (46)	2.29	α-helices: 2.05
BSA	2.52 ($\pm$ 0.12)	62.6	3.4 (45)	2.20	α-helices: 2.14
CON	2.80 ($\pm$ 0.14)	104	3.84 (47)	2.16	β-sheets: 2.50
IgG	2.94 ($\pm$ 0.07)	~160	5.51 (48)	1.77	β-sheets: 1.48
GFP	2.84 ($\pm$ 0.08)	25.8	2.48 (49)	1.91	β-barrel diameter: 2.40 (50)
LYS	2.57 ($\pm$ 0.14)	14.3	2.05 (46)	1.91	
CAS	2.21 ($\pm$ 0.06)	25	16 (51)	2.39	
aa-GFP	4.31 ($\pm$ 0.09)	0.075–0.204	—	1.85	
aa-BSA	—	0.075–0.204	—	1.81	

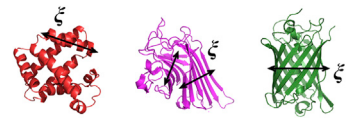

BP frequencies (ν_{BP}), obtained from NS data on dry powders at 170 K, are listed together with values of the correlation lengthscale, ξ, estimated using Eq. 5, the molecular mass, hydrodynamic radius (R_H), average diameter of the β-barrel, and average length of the α-helices or average width of β-sheets of the molecules. The last two parameters were obtained from the PDB structures of the proteins (1DWT; 3V03; 1LYZ; 2YZ4; 1IGT; and 1GFL). The uncertainties for ν_{BP} (reported in parentheses) were the errors provided by the fit (Eq. 4). (*Inset*) Cartoon representations of MYO, CON, and GFP show the correlation between ξ and the size of secondary structural units. To see the cartoon representations in color, go online.

aa-mixture of GFP is found at higher frequency than is the BP of the protein GFP. This observation indicates that the aa-mixture is a stiffer system relative to the folded protein of the same chemical composition. The example of small molecules of mono- and polyalcohols demonstrates the importance of hydrogen bond density, with the frequency of BP increasing at higher hydrogen bond densities (54). It is also known that the number of backbone H-bonds per residue is <1 for a folded protein (16), suggesting a potential increase of two H-bonds per residue from the carboxyl and amino groups that are free from the peptide backbone. In this way, we can attribute higher BP frequency in amino acid mixtures to an increase in the number and collective strength of H- bonds per residue.

This difference in rigidity is also supported by Brillouin LS measurements in the GHz frequency range, which show that the longitudinal sound velocities obtained for aa-GFP are higher than those observed for GFP in the entire temperature range investigated (100–295 K) (Fig. S4).

Finally, we want to make a brief comment regarding the BP feature in hydrated proteins. It has been observed (11,12,15,16,18) that the position of the BP in different proteins shifts to higher frequency upon hydration, reflecting strong protein-water hydrogen-bonding interactions, and a general increase of rigidity in the system. We demonstrated in our previous work that the trend of increased rigidity with protein secondary structure is preserved in the hydrated state (16). Moreover, both light and NS experiments (55,56) consistently demonstrate that the low-frequency vibrations in protein powders and solution show remarkable similarities. Therefore, the conclusions drawn for protein powders should be considered relevant to proteins in solution.

BP spectral shape

We now shift our focus to the discussion of the spectral shape of the BP for the proteins and amino acid mixtures studied. To analyze peak shape, we normalized the NS spectral density data to the frequency of the maximum (ν_{BP}) and to the intensity of the BP (I_{BP}). This is shown for all dry samples at 170 K in Fig. 4. Interestingly, in this presentation, the spectral shape of the BP appears to be universal for all the seven proteins and the aa-GFP mixture measured with NS. This observation is also valid for the spectra measured at different temperatures (170 K and 295 K; Fig. S7 *a*) and hydration levels (dry and $h = 0.4$, where h is the ratio between grams of water and grams of protein; Fig. S7 *b*).

This result suggests a universal origin of the BP in proteins. Chemical composition, connectivity of the constituent amino acids, 3D structure, and local rigidity do not appear to affect the spectral shape, but there are systematic differences in the peak position and amplitude.

A universal shape of the BP has also been reported for a series of oxide, chalcogenide, metallic, superionic, and low-molecular weight organic glasses (23–25). It was demonstrated that different chemical composition, chemical bond type (metallic or covalent), and short-range order of these various glass formers did not affect the spectral shape of the low-frequency vibrational density of states of glass formers. How do our observations of universal shape fit into the current understanding of the BP? Soft potential models assume that sound waves are coupled to local oscillators, which are produced by double-well-like soft potentials. The parameters of the soft potentials are chosen to have a broad statistical distribution predicting that local oscillator frequencies will follow $g(\nu) \propto \nu^4$ on the low-frequency side of the peak, and $g(\nu) \propto \nu$ on the high-frequency side. Structural-disorder models (36) predict the same $g(\nu) \propto \nu$ on the high-frequency side, whereas the low-frequency part of the peak comes from elastic scattering of soundlike waves by disorder in elastic constants of the medium, rather than from the anharmonic interactions. Unfortunately, our data do not provide enough information to validate these models, as relaxations of the proteins (quasielastic scattering) obscure a clear evaluation even at low temperature.

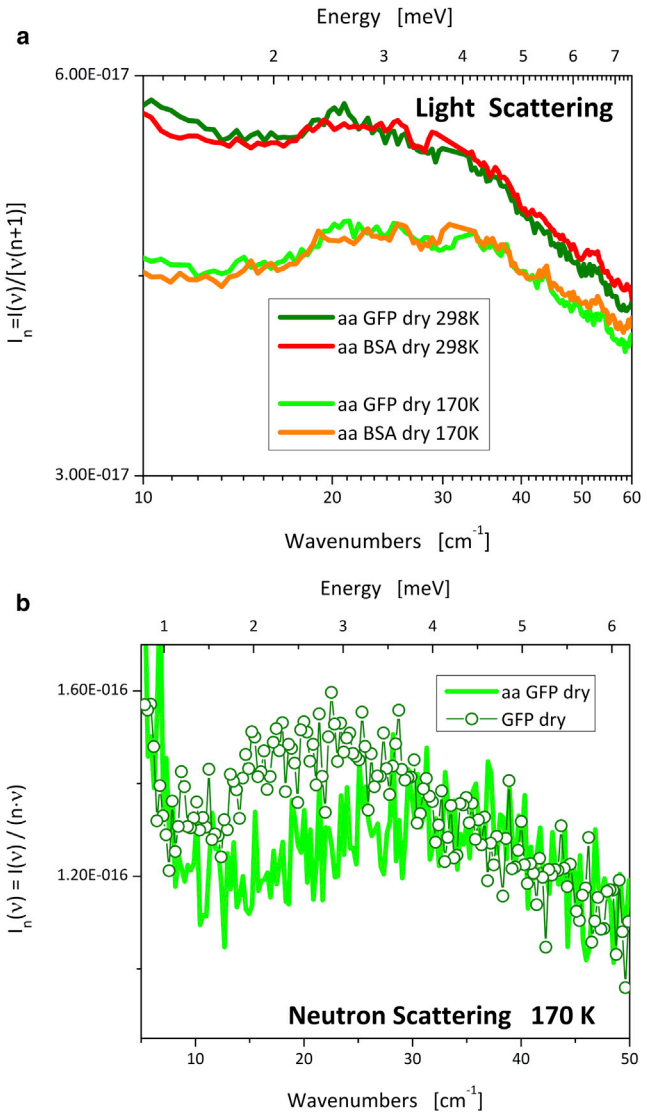

FIGURE 3 (*a*) Depolarized LS spectra of the BP region for dry aa-GFP and aa-BSA presented as the spectral density, I_n, at 170 K and 295 K. (*b*) NS I_n spectra of dry aa-GFP (*lines*) and GFP (*symbols*) at 170 K. To see this figure in color, go online.

Fig. 5 illustrates $g(\nu)/\nu^2$ from NS experiments in the ν/ν_{BP} coordinate for a selection of proteins in this work and glasses in previous publications (23,24,26). It is clear that the BP of proteins and glasses exhibit the same universal spectral shape upon normalization, indicating a common microscopic origin of the underlying dynamics. This suggests that the BP shape cannot be strongly associated with the specific chemical composition of the systems, but must be ascribed to more general features common to glasses and proteins. One such feature, recognized by different types of models, is the presence of elastic heterogeneities on the nanometer lengthscale. In fact, our observations of universal shape of the BP upon normalization are consistent with the framework proposed in nanoheterogeneity models. From this perspective, the BP is described as the collection of vibrations arising from heterogeneities in elastic constants within the glass with a characteristic lengthscale of a few nanometers. According to these models, the spectrum of the excess vibrational density of states is determined by the spatial distribution of fluctuations in the elastic constants of the amorphous structure. The universal shape of the spectral feature can be related to the universality of this distribution. The distribution can be modeled with a lognormal function (24). Assuming an acoustic-like nature of the BP vibrations, we can gain some understanding of the characteristic size or correlation lengthscale, ξ, of such nanoheterogeneities through the relation (39,42)

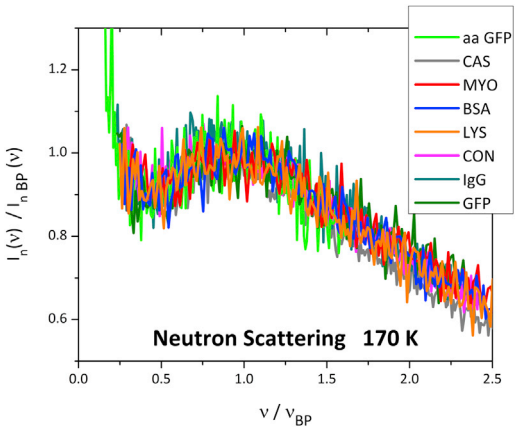

FIGURE 4 Universal shape of the normalized BP for the seven proteins and the aa-GFP mixture. The NS spectral densities were scaled to BP position and intensity. To see this figure in color, go online.

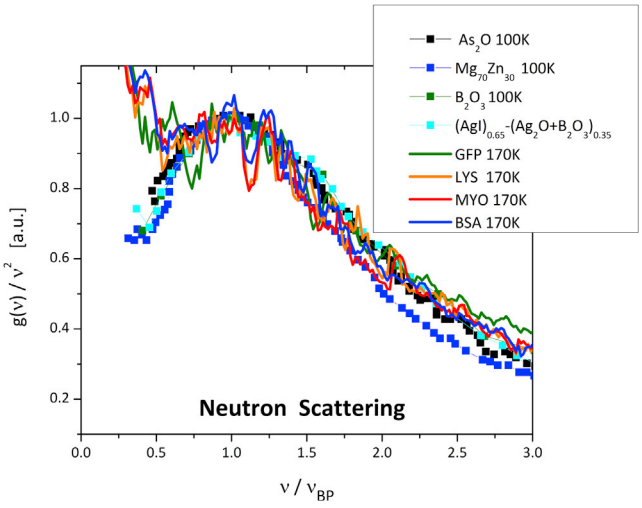

FIGURE 5 Universal shape of the reduced $g(\nu)/\nu^2$ for glasses and proteins. As_2O, $Mg_{70}Zn_{30}$, and $(AgI)_{0.65}$-$(Ag_2O+B_2O_3)_{0.35}$ spectra are from studies by Malinovsky and colleagues (23,24), and B_2O_3 spectra are from Engberg and Wischnewski (26). To see this figure in color, go online.

$$\xi = S \times \frac{c_T}{\nu_{BP}}, \quad (5)$$

where ν_{BP} is the BP frequency, c_T is the transverse sound velocity, and S is a constant defined by the shape and amplitude of the nanoscale heterogeneities.

By combining our measurements of sound velocity and the BP from LS (Supporting Material) as described in Perticaroli et al. (16), we applied the nanoheterogeneities model to all the proteins and aa-mixture samples to estimate this correlation lengthscale, ξ (Table 1). We do not exclude the potential validity of other interpretations of the BP. We have chosen to proceed using a heterogeneity model to obtain the physical lengthscale of elastic heterogeneities, which is a common feature across a wide range of different models (33,34,38–42).

Table 1 also provides a comparison between the sizes of the proteins and the average sizes of the secondary structure: length of the α-helices, size of β-sheets, and diameter of the β-barrel. As already mentioned (16), ξ does not scale with the size of the proteins. The correlation length obtained for BSA and MYO is very close to the average length of the α-helices, and the estimate of ξ for GFP is similar to the diameter of the β-barrel. We note that ξ in other β-structures seems to correspond to the width of the β-sheet (Table 1, *inset*). In fact, IgG, although larger than concanavalin A, is characterized by the narrowest β-sheets and presents a smaller ξ compared to CON, whose strands are arranged in wider sheets. We also notice that the softest disordered protein, CAS, has the largest correlation length, $\xi \sim 2.4$ nm, whereas the stiff H-bonded aa-mixtures have $\xi \sim 1.8$ nm. Finally, the correlation length of the mixed-motifs protein, lysozyme, probably results from the combination of all three secondary structural units forming the molecule, as we would expect to see in other mixed proteins. It is important to note that the dimensions of protein secondary structures agree well with the lengthscale predicted for nanoscopic heterogeneities. Beyond this, we again note the trend in the local rigidity of these secondary structures/nanoscopic heterogeneities, with β-structures appearing generically more rigid than α-structures, which are in turn more rigid than the unstructured regions (Fig. 2). This does tend to support the heterogeneity models, with proteins providing an excellent experimental system with well-defined nanometer-scale heterogeneities. However, recent studies of collective dynamics in GFP using coherent NS of fully deuterated GFP reveal that in-phase motions of secondary-structural elements contribute less than half of the scattered intensity at the BP (43). This folded protein differs from synthetic polymers and some molecular glass-forming materials, where coherent NS revealed strong in-phase collective motions of neighboring structural units in the low-frequency vibrational modes (19–22). This may relate to the lack of higher-order structure in these materials relative to the complex folded structure seen in proteins.

CONCLUSIONS

Our results provide insight into collective vibrations, illustrating the role of size and rigidity of the protein secondary structure in determining the timescale of such dynamics. We have analyzed the position and spectral shape of the BP in proteins as a function of secondary structure. We observe that the BP position is sensitive to the rigidity of the predominant secondary structure, i.e., random coil $<$ α-helix $<$ β-sheet. The subpicosecond collective vibrations in proteins, the so-called BP, occur on timescales associated with chemical barrier crossing and proton tunneling effects, and they play a crucial role in facilitating large conformational translations. Moreover, there is evidence that the spectral shape of the BP is universal not just among proteins, but among a wide range of glass formers. This is to our knowledge the first demonstration that the BP of proteins, amino acid mixtures, and glass formers potentially share a physical origin; independent of chemical composition. Our interpretation in terms of the nanoheterogeneities model illustrates the connection of the BP and secondary-structural elements such as α-helices and β-sheets. Our findings suggest that the BP in proteins behaves in a manner similar to that seen in glassy materials. This analysis connects the frequency of the collective low-frequency vibrational excitations in proteins to the size and rigidity of their secondary structure, similar to heterogeneity models, which predict that the properties of heterogeneities influence the BP in glasses.

These results contribute to the fundamental understanding of the interplay between protein structure and dynamics at the vibrational timescale. This observed relationship (β-sheets are more rigid than α-helices, which are more rigid than disordered proteins) is based on a clear experimental result. Going forward, this provides the community with time- and lengthscales of these motions of basic protein structures. Furthermore, there are tantalizing implications for those interested in the design and development of novel protein-based materials. Our findings may be useful in the engineering of bio-inspired structures using secondary structures as building blocks with specific mechanical rigidities to create new architectures that mimic and exceed the properties of biological systems.

SUPPORTING MATERIAL

Seven figures and references (57–63) are available at http://www.biophysj.org/biophysj/supplemental/S0006-3495(14)00506-2.

The authors thank the Spallation Neutron Source-User Chemistry Lab and Hugh O'Neill and Qiu Zhang for providing GFP. J.D.N. and S.P. designed and participated in all experiments, analyzed the data, and together with A.P.S. wrote the article. G.E. is the responsible instrument scientist at Cold Neutron Chopper Spectrometer and performed and supervised the NS measurements.

The authors acknowledge Department of Energy support through the EPSCoR program (grant DE-FG02–08ER46528) and the Scientific User Facilities Division, Office of Basic Energy Sciences, U.S. Department of

Energy. Oak Ridge National Laboratory facilities are sponsored by UT-Battelle, LLC, for the U.S. Department of Energy under contract No. DEAC05–00OR22725.

REFERENCES

1. Hay, S., and N. S. Scrutton. 2012. Good vibrations in enzyme-catalysed reactions. *Nat. Chem.* 4:161–168.
2. Silva, R. G., A. S. Murkin, and V. L. Schramm. 2011. Femtosecond dynamics coupled to chemical barrier crossing in a Born-Oppenheimer enzyme. *Proc. Natl. Acad. Sci. USA.* 108:18661–18665.
3. Schwartz, S. D., and V. L. Schramm. 2009. Enzymatic transition states and dynamic motion in barrier crossing. *Nat. Chem. Biol.* 5:551–558.
4. Kohen, A., R. Cannio, …, J. P. Klinman. 1999. Enzyme dynamics and hydrogen tunnelling in a thermophilic alcohol dehydrogenase. *Nature.* 399:496–499.
5. Balabin, I. A., and J. N. Onuchic. 2000. Dynamically controlled protein tunneling paths in photosynthetic reaction centers. *Science.* 290:114–117.
6. Vashisth, H., and C. Brooks, III. 2012. Conformational sampling of maltose-transporter components in Cartesian collective variables is governed by the low-frequency normal modes. *J. Phys. Chem. Lett.* 3:3379–3384.
7. Buehler, M. J. 2006. Nature designs tough collagen: explaining the nanostructure of collagen fibrils. *Proc. Natl. Acad. Sci. USA.* 103:12285–12290.
8. Ackbarow, T., X. Chen, …, M. J. Buehler. 2007. Hierarchies, multiple energy barriers, and robustness govern the fracture mechanics of α-helical and β-sheet protein domains. *Proc. Natl. Acad. Sci. USA.* 104:16410–16415.
9. Knowles, T. P., and M. J. Buehler. 2011. Nanomechanics of functional and pathological amyloid materials. *Nat. Nanotechnol.* 6:469–479.
10. Angell, C. A. 1995. Formation of glasses from liquids and biopolymers. *Science.* 267:1924–1935.
11. Diehl, M., W. Doster, …, H. Schober. 1997. Water-coupled low-frequency modes of myoglobin and lysozyme observed by inelastic neutron scattering. *Biophys. J.* 73:2726–2732.
12. Tarek, M., and D. J. Tobias. 2001. Effects of solvent damping on side chain and backbone contributions to the protein boson peak. *J. Chem. Phys.* 115:1607–1612.
13. Kurkal-Siebert, V., and J. C. Smith. 2006. Low-temperature protein dynamics: a simulation analysis of interprotein vibrations and the boson peak at 150 K. *J. Am. Chem. Soc.* 128:2356–2364.
14. Paciaroni, A., A. Orecchini, …, F. Sacchetti. 2008. Fingerprints of amorphous icelike behavior in the vibrational density of states of protein hydration water. *Phys. Rev. Lett.* 101:148104.
15. Nickels, J. D., H. O'Neill, …, A. P. Sokolov. 2012. Dynamics of protein and its hydration water: neutron scattering studies on fully deuterated GFP. *Biophys. J.* 103:1566–1575.
16. Perticaroli, S., J. D. Nickels, …, A. P. Sokolov. 2013. Secondary structure and rigidity in model proteins. *Soft Matter.* 9:9548–9556.
17. De Francesco, A., M. Marconi, …, A. Paciaroni. 2004. Picosecond internal dynamics of lysozyme as affected by thermal unfolding in nonaqueous environment. *Biophys. J.* 86:480–487.
18. Nakagawa, H., Y. Joti, …, M. Kataoka. 2008. Hydration affects both harmonic and anharmonic nature of protein dynamics. *Biophys. J.* 95:2916–2923.
19. Buchenau, U., A. Wischnewski, …, B. Frick. 1996. Is the fast process at the glass transition mainly due to long wavelength excitations? *Phys. Rev. Lett.* 77:4035–4038.
20. Engberg, D., A. Wischnewski, …, L. Torell. 1999. Origin of the boson peak in a network glass B_2O_3. *Phys. Rev. B.* 59:4053.
21. Sokolov, A. 1999. Vibrations at the boson peak: random-and coherent-phase contributions. *J. Phys. Condens. Matter.* 11:A213.
22. Sokolov, A. P., U. Buchenau, …, B. Frick. 1999. Brillouin and Umklapp scattering in polybutadiene: comparison of neutron and x-ray scattering. *Phys. Rev. E Stat. Phys. Plasmas Fluids Relat. Interdiscip. Topics.* 60:R2464–R2467.
23. Malinovsky, V., V. Novikov, …, M. Zemlyanov. 1990. Universal form of the low-energy (2 to 10 meV) vibrational spectrum of glasses. *Europhys. Lett.* 11:43–47.
24. Malinovsky, V., V. Novikov, and A. Sokolov. 1991. Log-normal spectrum of low-energy vibrational excitations in glasses. *Phys. Lett. A.* 153:63–66.
25. Malinovsky, V., and A. Sokolov. 1986. The nature of boson peak in Raman scattering in glasses. *Solid State Commun.* 57:757–761.
26. Engberg, D., A. Wischnewski, …, L. Torell. 1998. Sound waves and other modes in the strong glass former B_2O_3. *Phys. Rev. B.* 58:9087–9097.
27. Monaco, G., and V. M. Giordano. 2009. Breakdown of the Debye approximation for the acoustic modes with nanometric wavelengths in glasses. *Proc. Natl. Acad. Sci. USA.* 106:3659–3663.
28. Ruta, B., G. Baldi, …, G. Monaco. 2012. Acoustic excitations in glassy sorbitol and their relation with the fragility and the boson peak. *J. Chem. Phys.* 137:214502–214511.
29. Parshin, D. 1993. Soft potential model and universal properties of glasses. *Phys. Scripta.* 1993:180–185.
30. Gurevich, V., D. Parshin, and H. Schober. 2003. Anharmonicity, vibrational instability, and the Boson peak in glasses. *Phys. Rev. B.* 67:094203.
31. Parshin, D., H. Schober, and V. Gurevich. 2007. Vibrational instability, two-level systems, and the boson peak in glasses. *Phys. Rev. B.* 76:064206.
32. Chumakov, A. I., G. Monaco, …, P. Piekarz. 2011. Equivalence of the boson peak in glasses to the transverse acoustic van Hove singularity in crystals. *Phys. Rev. Lett.* 106:225501.
33. Lubchenko, V., and P. G. Wolynes. 2003. The origin of the boson peak and thermal conductivity plateau in low-temperature glasses. *Proc. Natl. Acad. Sci. USA.* 100:1515–1518.
34. Stevenson, J. D., J. Schmalian, and P. G. Wolynes. 2006. The shapes of cooperatively rearranging regions in glass-forming liquids. *Nat. Phys.* 2:268–274.
35. Grigera, T. S., V. Martín-Mayor, …, P. Verrocchio. 2003. Phonon interpretation of the 'boson peak' in supercooled liquids. *Nature.* 422:289–292.
36. Schirmacher, W., G. Ruocco, and T. Scopigno. 2007. Acoustic attenuation in glasses and its relation with the boson peak. *Phys. Rev. Lett.* 98:025501.
37. Taraskin, S. N., Y. L. Loh, …, S. R. Elliott. 2001. Origin of the boson peak in systems with lattice disorder. *Phys. Rev. Lett.* 86:1255–1258.
38. Sokolov, A., R. Calemczuk, …, E. Duval. 1997. Low-temperature anomalies in strong and fragile glass formers. *Phys. Rev. Lett.* 78:2405–2408.
39. Boukenter, A., B. Champagnon, …, J. Serughetti. 1986. Low-frequency Raman scattering from fractal vibrational modes in a silica gel. *Phys. Rev. Lett.* 57:2391–2394.
40. Leonforte, F., R. Boissiere, …, J.-L. Barrat. 2005. Continuum limit of amorphous elastic bodies. III. Three-dimensional systems. *Phys. Rev. B.* 72:224206.
41. Duval, E., A. Mermet, and L. Saviot. 2007. Boson peak and hybridization of acoustic modes with vibrations of nanometric heterogeneities in glasses. *Phys. Rev. B.* 75:024201.
42. Duval, E., A. Boukenter, and T. Achibat. 1990. Vibrational dynamics and the structure of glasses. *J. Phys. Condens. Matter.* 2:10227.
43. Nickels, J. D., S. Perticaroli, …, A. P. Sokolov. 2013. Coherent neutron scattering and collective dynamics in the protein, GFP. *Biophys. J.* 105:2182–2187.
44. Ehlers, G., A. A. Podlesnyak, J. L. Niedziela, E. B. Iverson, and P. E. Sokol. 2011. The new cold neutron chopper spectrometer at the

Spallation Neutron Source: design and performance. *Review of Scientific Instruments.* 82: 085108–085108–085106.

45. Suezaki, Y., and N. Gö. 1975. Breathing mode of conformational fluctuations in globular proteins. *Int. J. Pept. Protein Res.* 7:333–334.

46. Brown, K. G., S. C. Erfurth, …, W. L. Peticolas. 1972. Conformationally dependent low-frequency motions of proteins by laser Raman spectroscopy. *Proc. Natl. Acad. Sci. USA.* 69:1467–1469.

47. Mikol, V., E. Hirsch, and R. Giegé. 1990. Diagnostic of precipitant for biomacromolecule crystallization by quasi-elastic light-scattering. *J. Mol. Biol.* 213:187–195.

48. Jøssang, T., J. Feder, and E. Rosenqvist. 1988. Photon correlation spectroscopy of human IgG. *J. Protein Chem.* 7:165–171.

49. Potma, E. O., W. P. de Boeij, …, D. A. Wiersma. 2001. Reduced protein diffusion rate by cytoskeleton in vegetative and polarized dictyostelium cells. *Biophys. J.* 81:2010–2019.

50. Brejc, K., T. K. Sixma, …, S. J. Remington. 1997. Structural basis for dual excitation and photoisomerization of the *Aequorea victoria* green fluorescent protein. *Proc. Natl. Acad. Sci. USA.* 94:2306–2311.

51. Aguié-Béghin, V., P. Sausse, …, R. Douillard. 2008. Polyphenol-β-casein complexes at the air/water interface and in solution: effects of polyphenol structure. *J. Agric. Food Chem.* 56:9600–9611.

52. Wright, P. E., and H. J. Dyson. 1999. Intrinsically unstructured proteins: re-assessing the protein structure-function paradigm. *J. Mol. Biol.* 293:321–331.

53. Schirò, G., C. Caronna, F. Natali, M. M. Koza, and A. Cupane. 2011. The "protein dynamical transition" does not require the protein polypeptide chain. *The journal of physical chemistry letters.* 2:2275–2279.

54. Yamamuro, O., K. Harabe, …, T. Kanaya. 2000. Boson peaks of glassy mono- and polyalcohols studied by inelastic neutron scattering. *J. Phys. Condens. Matter.* 12:5143–5154.

55. Perticaroli, S., L. Comez, …, A. Morresi. 2010. Broadband depolarized light scattering study of diluted protein aqueous solutions. *J. Phys. Chem. B.* 114:8262–8269.

56. Marconi, M., E. Cornicchi, …, A. Paciaroni. 2008. Comparative study of protein dynamics in hydrated powders and in solutions: a neutron scattering investigation. *Chem. Phys.* 345:224–229.

57. Luo, G., Q. Zhang, …, H. O'Neill. 2009. Characterization of sol-gel-encapsulated proteins using small-angle neutron scattering. *ACS Appl. Mater. Interfaces.* 1:2262–2268.

58. Michael Byler, D., H. M. Farrell, Jr., and H. Susi. 1988. Raman spectroscopic study of casein structure. *J. Dairy Sci.* 71:2622–2629.

59. Khodadadi, S., A. Malkovskiy, …, A. P. Sokolov. 2010. A broad glass transition in hydrated proteins. *Biochim. Biophys. Acta.* 1804:15–19.

60. Smith, J., S. Cusack, …, M. Karplus. 1986. Inelastic neutron scattering analysis of low frequency motion in proteins: a normal mode study of the bovine pancreatic trypsin inhibitor. *J. Chem. Phys.* 85:3636–3654.

61. Balog, E., T. Becker, …, J. C. Smith. 2004. Direct determination of vibrational density of states change on ligand binding to a protein. *Phys. Rev. Lett.* 93:028103.

62. Squires, G. L. 2012. Introduction to the Theory of Thermal Neutron Scattering. Cambridge University Press, Cambridge, United Kingdom.

63. Azuah, R. T., L. R. Kneller, …, R. M. Dimeo. 2009. DAVE: a comprehensive software suite for the reduction, visualization, and analysis of low energy neutron spectroscopic data. *J. Res. Natl. Inst. Stand. Technol.* 114:341–358.